Atomization of liquid film in annular gas-liquid flow: Study of tracks of droplets at the initial stages using LIF system

S.V. Alekseenko[1,2], A.V. Cherdantsev[1,2*], D.M. Markovich[1,2] and A.V. Rabusov[1,2]
[1] Kutateladze Institute of Thermophysics, Novosibirsk, Russian Federation
[2] Novosibirsk State University, Novosibirsk, Russian Federation
aleks@itp.nsc.ru, cherdantsev@itp.nsc.ru, dmark@itp.nsc.ru, arabusov@gmail.com

Abstract

Recently high-speed modification of laser-induced fluorescence technique was applied to studying the wavy structure of liquid film in annular flow either with or without liquid entrainment. Dynamics of fast and slow ripples, covering, respectively, surface of disturbance waves and surface of the base film between them, was described qualitatively. In present paper the laser-induced fluorescence technique was used for investigation of droplets dynamics in annular two-phase flow. It was found that the technique can be used for simultaneous studying of the disturbance waves, ripples and entrained droplets. In particular, velocity and size of droplets right after the act of entrainment were measured. It was shown that coalescence of disturbance waves doesn't make essential contribution to the total entrainment. Process of droplets impingement into the ripples on the base film and subsequent secondary entrainment of droplets was observed and described.

1. Introduction

Gas-liquid flow regime when liquid travels as a film along channel walls, sheared by high-velocity gas stream, is termed as annular flow. It is well-known that the film surface in annular flow is covered by waves of the two types: disturbance waves with height several times greater than the mean film thickness and small-scale ripple waves. The two types of waves differ greatly in velocity, lifetime, longitudinal size, etc. One of the most interesting phenomena in annular flow is the atomization of liquid film. As the result of atomization, part of liquid travels as droplets in the core of gas stream. Waves and atomization were investigated intensively during the last fifty years, since they exert essential influence on the heat and mass transfer as well on the pressure drop in annular flow.

Different mechanisms of liquid film atomization were proposed by researchers:

1) Disruption of ripple waves travelling over the disturbance waves by the gas shear [1], also known as 'Kelvin-Helmholtz lifting' (KHL) mechanism.

2) Shearing-off disturbance waves crests [2], also known as 'roll waves stripping' (RWS) mechanism.

3) Disturbance waves undercutting [2].

4) Coalescence of disturbance waves [3].

5) Secondary entrainment after impingement of depositing droplet at the film surface.

6) Entrainment after bursting of bubbles, entrapped by liquid [2].

Direct investigation of the act of entrainment is complicated by a number of reasons like:

1) Small spatial and temporal scales of process, requiring high spatial and temporal resolution;

2) Large size of spatial and temporal domains that should be investigated (the size is large due to high velocity of waves and, especially, droplets);

3) Complicated structure of liquid film that could distort the observations.

Disturbance waves and sometimes ripples were investigated by the large number of researchers who measured the characteristics of the waves. In particular, characteristics like velocity, frequency, amplitude, length and spacing were measured by different researchers who employed various measurement techniques (see [4-8]). In our recent work [9] spatial and temporal evolution of disturbance waves and ripples was investigated using high-speed laser-induced fluorescence technique. It was shown that all the ripples are generated at the rear slopes of disturbance waves. From there ripples may move either faster or slower than disturbance waves. In the former case, 'fast' ripples travel over the disturbance waves and finally they are disrupted by the gas shear into droplets. This observation confirms KHL-mechanism, based on observations of [1].

Another approach was to investigate properties of droplets (concentration, velocity and size distribution, etc.). Researchers used conductance methods [10], drop sampling methods [11], laser axial view technique[12], diffraction technique [13] etc. Normally the measurements were performed after taking out the liquid film to

*Corresponding author: cherdantsev@itp.nsc.ru

avoid optical distortions. Size of droplets was shown to be described by log-normal upper-limit distribution, and the average velocity of droplets was about 80% of the superficial gas velocity [4].

Authors of [12] measured the lateral component of droplets velocity. Axial-viewing technique was used to obtain projections of trajectories of droplets on the plane, orthogonal to the axis of flow direction. Due to diffraction problems only heavy droplets (with diameter of about 0.2 mm and larger) were investigated. It was established that heavy droplets move in this plane with approximately constant velocity (average value of 0.86 m/s for gas velocity 24 m/s), whereas smaller droplets were supposed to be susceptible to the action of turbulent pulsations of the gas, and their movement is governed rather by diffusion-like processes.

This paper is the most close to the present paper, since it is devoted to investigation of motion of droplets right after entrainment act. In present work we analyze the tracks of large droplets. These tracks were obtained rather unexpectedly by the LIF-technique, developed for studying the liquid film structure. The obtained experimental material allows us to study the waves and droplets simultaneously, which is useful for better understanding entrainment phenomenon. We focus on the initial stages of droplets evolution, attempting to 'approach' as close as possible to the act of entrainment.

Nomenclature

d – pipe diameter, m;
h – local film thickness, mm;
q – volumetric liquid flow rate, m^3/s;
t – time, s;
t_e – exposure, s;
x – longitudinal position, m;
x_l – position of left (upstream) border of a droplet;
x_r – position of right (downstream) border of a droplet;
D – droplet longitudinal size;
Re – liquid Reynolds number, $Re=q/\pi d\nu$;
Re_g – gas Reynolds number, $Reg=Vg*d/\nu_g$;
U_{gl} – relative velocity of gas $U_{gl}=V_g-V_{dw}$;
V_d – velocity of a droplet, m/s;
V_{dw} – velocity of disturbance wave, m/s;
Vg – superficial gas velocity, m/s;
σ – surface tension of liquid, kg/s^2;
ρ_g – gas density, kg/m^3;
ν – kinematical viscosity of liquid, m^2/s;
ν_g – kinematical viscosity of gas, m^2/s;

2. High-speed LIF-technique and wavy structure of liquid film in annular flow

Experiments were performed in downward annular flow, which was organized in Plexiglas tube with inner diameter d=15 mm. Liquid was introduced as a film through ring-slot distributor; gas (air) entered the tube through coaxial tube of slightly smaller diameter (Fig. 1, left). Water and two water-glycerol solutions with kinematical viscosities $\nu=1.5$ and $1.9*10^{-6}$ m^2/s were used as working liquids. Liquid Reynolds numbers ($Re=q/\pi d\nu$, where q is volumetric liquid flow rate) varied in the range 142-350, and superficial gas velocity Vg varied in the range of 18-70 m/s.

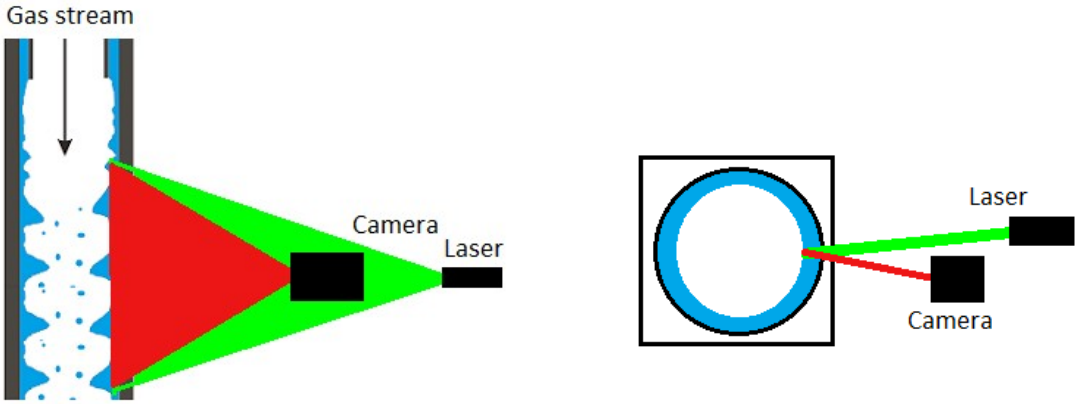

Figure 1 Sketch of flow along with scheme of the inlet section and layout of laser and camera: side view (left) and top view (right).

Laser-induced fluorescence technique was used to measure local film thickness. Fluorescent matter -Rhodamin-6G - was dissolved in liquid in low (10-20 mg/l) concentration. Longitudinal section of a pipe was enlightened by vertical laser sheet to excite the fluorescent light (Fig. 1). Local brightness of this light (measured by high-speed CCD-camera) was converted into local film thickness using calibration curve.

Camera frame rate was 10 kHz. Exposure varied from 30 to 70 μs depending on flow conditions. Spatial resolution (area, seen by a single pixel) was 0.2 mm in both directions. Measurements were performed at the distance of 50 cm below the inlet. Each 'frame' of camera represented instantaneous distribution of local film thickness over the length of 12 cm. 40 thousand such distributions were obtained for each regime point, giving 4 seconds of film thickness evolution.

Figure 2 shows an example of spatial and temporal behaviour of waves on liquid film. Brightness of image is directly proportional to the local film thickness. Vertical axis corresponds to time (total time-length of the image is 35 ms), horizontal axis – to the longitudinal distance (total length – 12 cm). Flow direction is from left to right. Disturbance wave can be seen here as a wide bright band beginning in the lower left corner. It crosses the image with velocity equal to

$$V_{dw} = \frac{\Delta x}{\Delta t} = \frac{0.09m}{0.035s} = 2.6\frac{m}{s}$$

Small fragment of another disturbance wave can be seen in the upper left corner. Base film between disturbance waves is covered by slow ripple waves that are generated at the back slopes of disturbance waves. New-generated slow ripples gradually decelerate; after that they travel along the base film with constant low velocity. Finally they are absorbed by the following disturbance wave. Surface of disturbance waves is covered by the fast ripples. Amplitude of the fast ripples is obviously overestimated by the LIF-technique. Most likely this happens due to refocusing of the laser light, reflected from liquid-gas surface. Nonetheless, behaviour of fast ripples in space and time, as well as their frequency, velocity and longitudinal size still can be investigated.

The fast ripples are also generated at the back slopes of disturbance waves, but they travel faster than those, and, finally, disappear. Comparison of this picture to the observations of [1] leads us to conclude that the disappearance occurs due to disruption of the fast ripple by the gas shear into tiny droplets that are entrained into the core of gas stream.

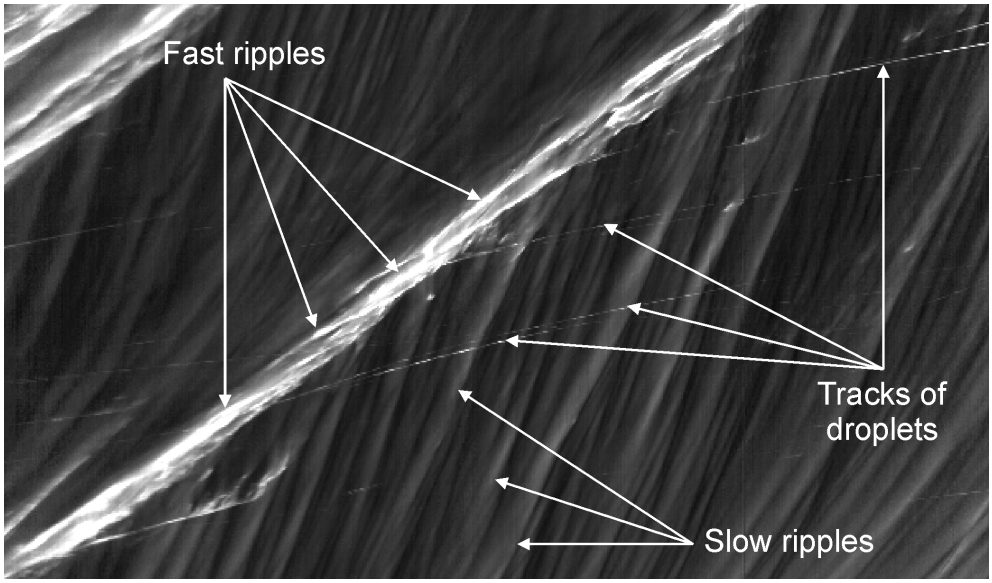

Figure 2 Spatial and temporal evolution of liquid film thickness. Disturbance waves, fast and slow ripples and tracks of entrained droplets are shown. Water, Re=220, Vg=27 m/s.

3. Application of LIF-technique to studying the droplets dynamics

Though the technique was aimed for film thickness measurements, some additional structures different from waves can be observed in the spatio-temporal surfaces of film thickness. Such structures represent high-velocity trajectories of objects looking like 'waves' of small longitudinal size and high amplitude. Evidently, we see the droplets, which travel along the investigated section of the pipe (total width of the investigated section was 0.2 mm) not far from the film surface.

Such trajectories do not appear in no-entrainment conditions. In entrainment conditions the most part of trajectories begins at the fronts of the disturbance waves (Fig. 2). Indeed, droplets are normally entrained from

disturbance waves (see Introduction). Newborn droplet normally moves with slight acceleration, but the initial velocity is already much greater than that of disturbance waves and fast ripples. One could speak about initial momentum, obtained by a droplet in process of disruption of the fast ripple. This corresponds to the observations of [12].

The trajectories normally do not interact to the slow ripples covering the base film (except for the case of droplet deposition on the base film, which will be discussed in section 4.3). Sometimes trajectories begin not only from disturbance waves or after the droplet impingement, but also 'from nowhere'. The same is true for the endings of trajectories. It is supposed to happen due to existence of small lateral velocity component, causing a droplet to enter (or exit) the narrow area of measurements. Due to narrow lateral size of the area of measurements, many droplets can't be seen even if the phenomenon, causing entrainment of the droplet, is visible in the area of measurements. At the same time, we can often see the droplets, moving over the whole investigated longitudinal distance (12 cm) without disappearance. Sometimes they can even fly over the disturbance waves without interaction.

Using this technique, we, obviously, can see only rather large drops. The first reason of this is relatively low spatial resolution. Spatial resolution of 0.2 mm satisfies the requirements for studying waves on liquid film, but not for studying the small droplets. The large size of the area, seen by single pixel (0.2*0.2 mm) leads to averaging the images of small droplets over this area, decreasing the signal and making detection more difficult. Detection of trajectories of small droplets is also expected to be complicated by the fact that small droplets are more susceptible to the action of turbulent pulsations in the gas phase. As the result, they are expected not to move along ballistic trajectories (see [12]).

Normally, the local peak of brightness, induced by a droplet, is expected to be rather high: first, the size of droplets is rather large in comparison to the base film thickness, and second, the laser light, reflected from the inner surface of a droplet, can be refocused inside the droplet, increasing local brightness. At the same time, droplets moving far from the liquid surface are expected to be less bright, since they are out of focus of the camera. E.g., in Fig 3(a) the level of signal of a droplet (three peaks between x=20 and 23 mm, corresponding to three time moments) is comparable to the level of fast ripples on disturbance waves (disturbance wave is located between x=0 and x=10 mm). Fig 3(b) shows the droplet in three time moments in larger scale.

We developed semi-automatic algorithm of data processing, allowing us to measure the main characteristics of observed droplets: average velocity, acceleration and longitudinal size (equal to diameter if a droplet is spherical). At the beginning, spatial and temporal coordinates of initial and final points of trajectory were registered manually (only the initial part of a trajectory was processed). Average velocity of droplets was then calculated. After that the spatial coordinates of the droplet were found automatically at every time moment. Algorithm was searching for the point of maximum intensity in a small range of distance around the expected position of droplet, as if it moved with constant average velocity. The width of the range could reach up to 20 pixels (4 mm) at the middle part of the trajectory, becoming narrower closer to the border points, since they were found manually. For very curved trajectories number of manually selected points could be increased to 3 or 4. The obtained trajectory was approximated by the quadratic equation, which allowed rough estimation of the average acceleration of droplets. For this purpose, only the longest trajectories were taken into account.

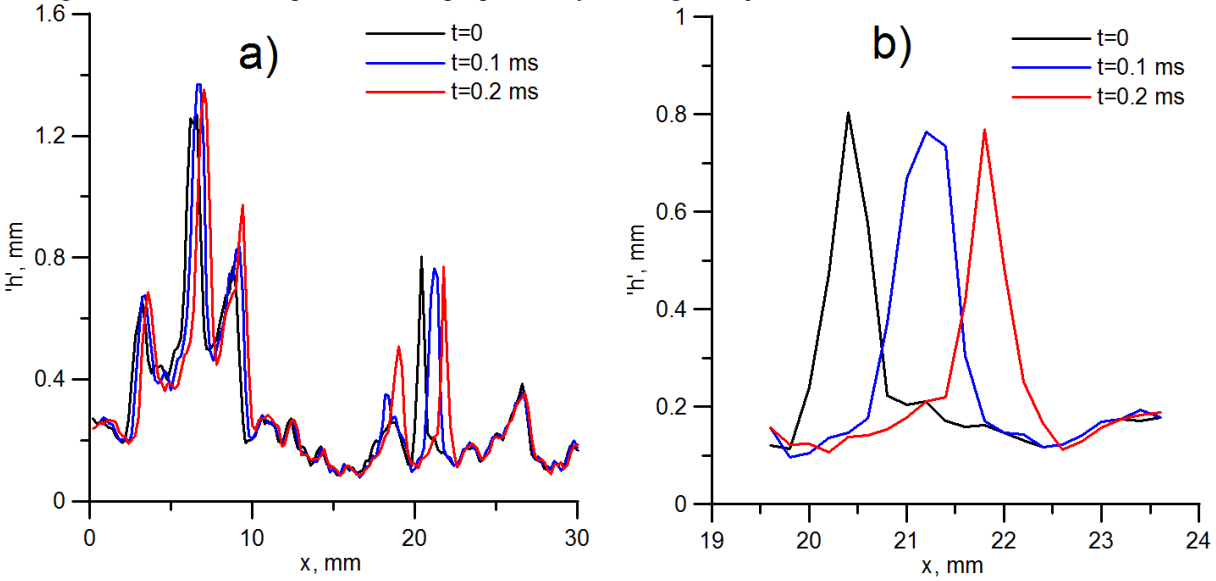

Figure 3 LIF-image film surface and a droplet in three subsequent time moments: disturbance wave and a droplet (a); the droplet in large scale (b). Water, Re=220, Vg=27 m/s.

To measure the size of droplets, each obtained trajectory was additionally processed. In every time moment vicinity of the maximum was compared to the profiles of film surface in neighbouring time moments (Figure 3 (b)). Left border of the droplet x_l was determined as the point where the local 'thickness' $h(x_l,t)$ satisfied to:

$$h(x_l,t) < h(x_l + 0.2mm, t + 0.1ms) * 1.1 \quad (1)$$

The right border x_r was determined in the same manner with change of sign in both time and space shifts. This method of measurement is based on essential difference in velocities of droplet and slow ripples. The height of a slow ripple in the same phase (shifting by 0.2 mm per 0.1 ms roughly corresponds to the observed velocity of slow ripples) is expected not to change essentially over the short time interval. Though, diameter of a droplet is not equal to x_r-x_l, since blurring of signal due to rather large exposure t_e (varying from 30 to 70 μs for different flow regimes) should also be taken into account.

$$D = x_r - x_l - t_e * V_d \quad (2)$$

To minimize the influence of errors on obtained diameter of a droplet, median value of diameters, registered in all time moments, was taken into account. An example of a droplet image in three neighbouring time moments is given in Figure 3 (b). For not so bright droplets condition doesn't work well, and they were not taken into account.

4. Results.

The results are presented in accordance to the mechanisms of entrainment, listed in the Introduction section, excluding the following:

1) Mechanism of waves undercutting, according to its description, is expected to take place in upward flow at low qualities. This is not the case, regarded in present experiment.

2) Spatial resolution is not enough to resolve the process of bubbles bursting, whether it takes place or not. Using our system, we are able to distinguish large bubbles (and they will be mentioned further), but their possible contribution to entrainment is out of ability of present state of the measuring system.

3) We didn't observe any events of film and droplets evolution that would satisfy the description of the 'roll waves stripping' mechanism. The statement that RWS mechanism doesn't take place at all needs stronger argumentation. For now we will just not discuss this mechanism further in present paper.

4.1. Kelvin-Helmholtz lifting mechanism

Figure 4 shows dependence of initial velocity (a) and size (b) of droplets. Algorithm of data processing is described in section 3. Only the droplets with trajectories, beginning at the disturbance waves, were processed. For each regime point not less than 30 (normally – 50-60) droplets were processed. It can be seen that the initial velocity of droplets is more than two times larger than the velocity of disturbance waves, and 4-5 times lower than the superficial gas velocity. Velocity of droplets grows approximately linearly with increasing gas velocity.

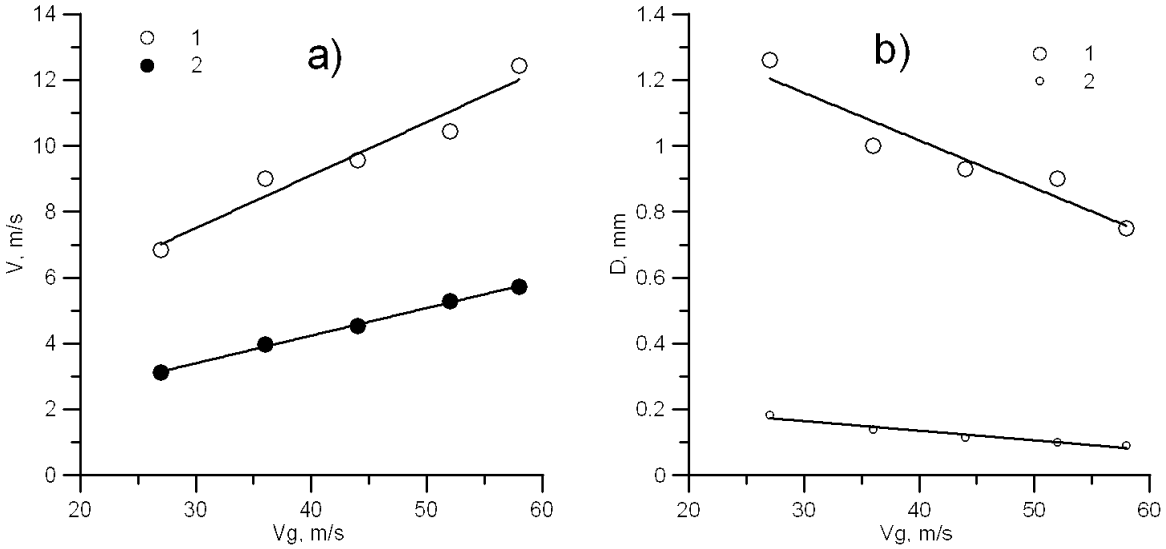

Figure 4 Velocity and size of newborn droplets. Water, Re=350. a) 1 - initial velocity of droplets; 2 - velocity of disturbance waves. b) 1- size of newborn droplets; 2 - prediction of droplets diameter by [10].

Size of droplets is unexpectedly large (of order of 1 mm). Increase in gas velocity leads to decreasing the initial size of droplets. In the same plot prediction of initial size of droplets by [10] is given as:

$$D = 0.0112\left(\frac{d\sigma}{0.023\,\mathrm{Re}_g^{-0.2}\,\rho_g U_{gl}^{\,2}}\right)^{0.5}$$

Here σ is surface tension, Re_g – gas Reynolds number, ρ_g – gas density and U_{gl} – relative velocity of gas. Experimental values are much larger than predicted values. Possible explanation of the discrepancy consists in size difference between the droplets that are just entrained (experimental values) and developed droplets, taken independently on waves. We assume that the large newborn droplets undergo secondary atomization process, i.e., they are depleted into smaller ones by the gas shear, and there were these smaller droplets which were measured and correlated by [10].

4.2. Disturbance waves coalescence mechanism.

Disturbance waves tend to coalesce due to scatter in velocity of individual waves. Number of coalescence acts is large near the inlet, and it gradually decreases with longitudinal distance as well as the number of disturbance waves. According to [3], when a faster wave overtakes slower preceding wave, they form a new wave with velocity of the faster wave. The volume of liquid, carried by the slower wave is supposed to be totally entrained into the core of gas stream. Under this hypothesis, authors of the paper [3] estimated contribution of this mechanism to be up to half of total entrainment.

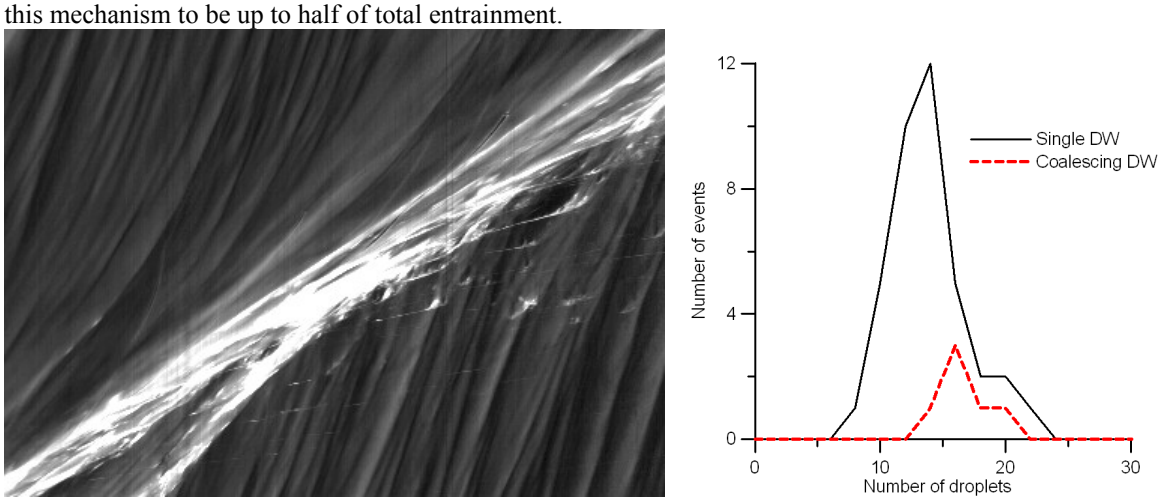

Figure 5. Left: Coalescence of two disturbance waves. Time length: 31 ms, total distance: 9 cm. Water, Re=142, Vg=27 m/s. Right: Comparison of number of droplets, entrained from single disturbance waves and from coalescing disturbance waves.

Using high-speed LIF visualization, it is possible to check this hypothesis. Figure 5 (left) shows an example of coalescence act. The resulting wave really travels with approximately the same speed as the faster wave did, but it is hard to affirm that all the other properties remain the same. Moreover, no outstanding number of droplets is seen after the coalescence (compare to Figure 2). We measured the average number of droplets, generated by a single disturbance wave and compared it to the number of droplets, generated by coalescing waves. The data are presented in Figure 5 (right) in the form of distributions of waves by the number of generated droplets. It can be seen that, though number of entrained droplets after coalescence is slightly larger than without it, no essential increase in number of droplets is observed.

Thus, the preliminary conclusion here is that the process of coalescence of disturbance waves is described by more complex scenario than it was supposed in [3], and that there is no outstanding contribution of this phenomenon into total entrainment.

4.3. Droplet impingement mechanism

Trajectory of a droplet may end at the base film (usually, at a slow ripple wave), accompanied by splashing of liquid (e.g., event 1in the upper part of Figure 6). The slow ripple in this case is essentially deformed by the impinging droplet: kind of cavern appears on the rear side, and there appears a deformation with very high curvature, leading to essential overestimation of its amplitude (event 2 in the upper part of Figure 6).

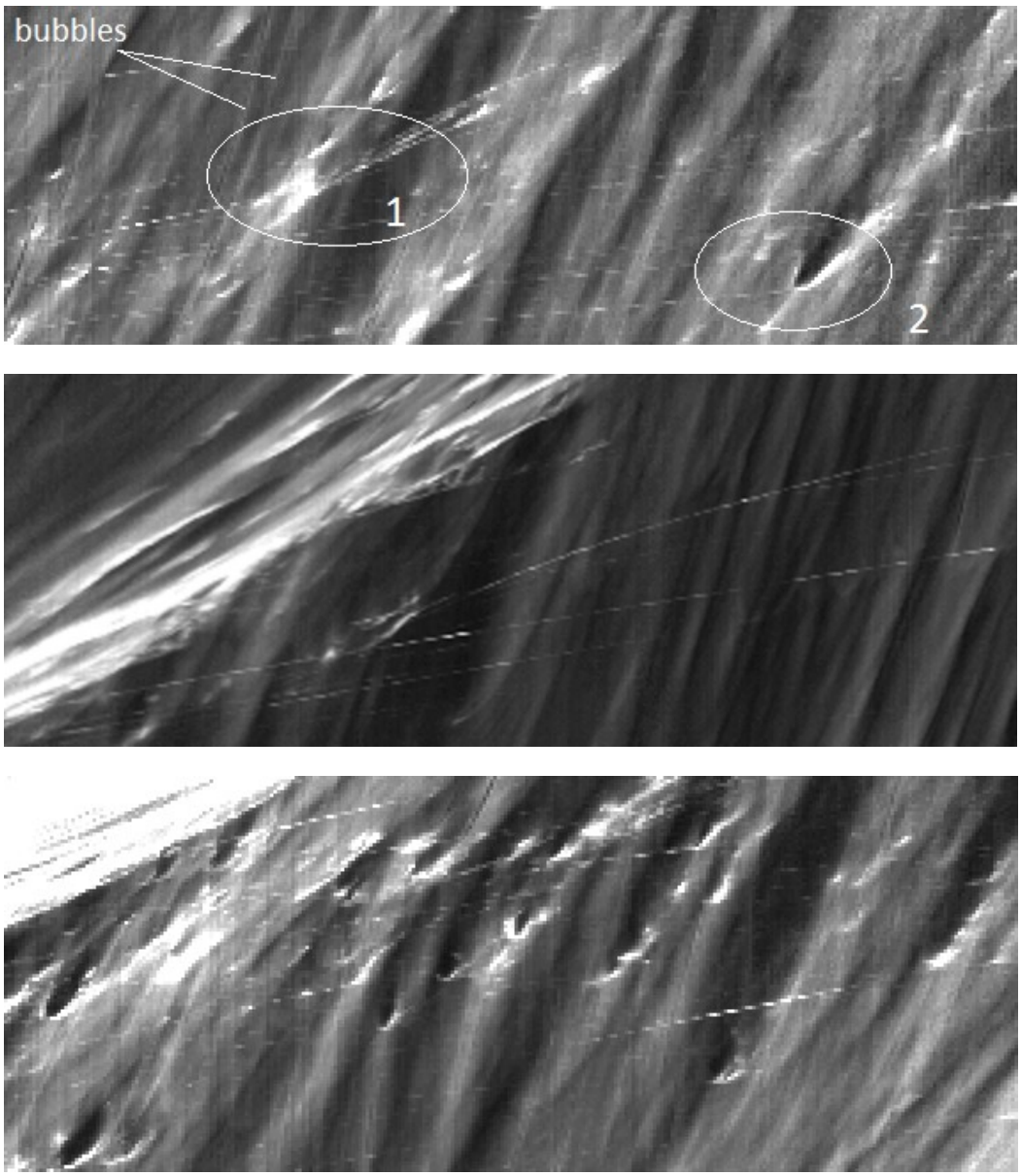

Figure 6 Deposition of droplets onto the base film and secondary entrainment. Re=142, Vg=27 m/s. Top and bottom: $\nu=1.9*10^{-6}$ m^2/s; middle: $\nu=1.15*10^{-6}$ m^2/s.

Sometimes, low-velocity trajectories with dark centre and bright borders are observed in experimental data. These structures the most likely represent large bubbles, entrapped by the liquid film (two bubbles are indicated in the upper part of Figure 6). We note that the trajectories of many bubbles appear after the event of droplet impingement.

In some cases, different droplets appear after the splash, moving with noticeable acceleration. The acceleration was measured for several droplets for one regime point (water, Re=350, Vg=27 m/s), and its average value was about 300 m/s^2. Rough estimation of the acceleration of a droplet by the turbulent drag force gave close results. It is interesting that the initial droplet doesn't necessarily disappear after impinging into the slow ripple and even after causing the secondary entrainment phenomenon (the middle part of Figure 6).

Number of droplets, directly impacting on the base film right after inception, can be very large (see the large number of 'caverns' in Figure 6, bottom). This should be taken into account in physically-based models, predicting the rate of entrainment.

5. Summary and Conclusions

The laser-induced fluorescence technique was used for investigation of droplets dynamics in annular two-phase flow. It was found that the technique can be used for simultaneous studying of the disturbance waves, ripples and entrained droplets. In particular, velocity and size of droplets right after the act of entrainment were measured. It was shown that the velocity of droplets is about two times larger than that of disturbance waves and

4-5 times lower than superficial gas velocity. Size of droplets is of order of 1 mm, and it decreases with gas velocity. It was shown that coalescence of disturbance waves doesn't make essential contribution to the total entrainment. Process of droplets impingement into the ripples on the base film and subsequent secondary entrainment of droplets was observed and described.

Development of the method is required in the nearest future. First, three-dimensional LIF approach should be used instead of the two-dimensional one. That means that not only longitudinal, but also circumferential coordinate should be resolved. Second, spatial and temporal resolution should be increased. Third, higher degree of automation of data processing algorithm should be developed.

Acknowledgements

The work was supported by Russian President (grants MK-115.2011.8 and NSh-6686.2012.8) and Russian Foundation for Basic Research (grant 10-08-01145a).

References

[1] Woodmansee, D.E. and Hanratty, T.J. *Chemical Engineering Science* 24: 299-307 (1969)
[2] Ishii, M. And Grolmes, M.A. *AIChE Journal* 21: 308-318 (1975)
[3] Wilkes, N.S., Azzopardi, B.J. and Thompson, C.P. *International Journal of Multiphase Flow* 9: 383-398 (1983)
[4] Azzopardi, B.J. *International Journal of Multiphase Flow* 23 Suppl.: 1-53 (1997)
[5] Han, H., Zhu, Zh. and Gabriel, K. *Nuclear Engineering and Design* 236: 2580–2588 (2006).
[6] Sawant, P., Ishii, M., Hazuku, T., Takamasa, T. and Mori, M. *Nuclear Engineering and Design* 238: 3528–3541 (2008)
[7] Belt, R.J., Van't Westende, J.M.C., Prasser, H.M. and Portela L.M. *International Journal of Multiphase Flow* 36: 570–587 (2010)
[8] Schubring, D., Shedd, T.A. and Hurlburt, E.T. *International Journal of Multiphase Flow* 36: 385–396 (2010).
[9] Alekseenko, S.V., Antipin, V.A., Cherdantsev, A.V., Kharlamov, S.M. and Markovich, D.M. *Physics of Fluids* 21: 061701–061704 (2009).
[10] Tatterson, D.F., Dallman, J.C. and Hanratty, T.J. *AIChE Journal*, 23: 68-76 (1977)
[11] Lee, E.H., NO, H.C., Yoo, S.H., Lee, K.W. and Song, C.-H. *Nuclear Engineering and Design* 240: 1795–1802 (2010)
[12] James, P.W., Hewitt, G.F. and Whalley, P.B. *IntTopical Meeting on Nuclear Reactor Thermal Hydraulics*. 2: 1484-1503 (1980).
[13] Alamu, M.B. and Azzopardi, B.J. *Nuclear Engineering and Design* 241: 5079–5092 (2011)